

# Research on trigger technology of MRPC TOF-PET system and imaging results of $^{22}\text{Na}$ radioactive source

---

Jianing Liu,<sup>a</sup> Yuelei Ma,<sup>b,c</sup> Ziyang Chen,<sup>a</sup> Zhenyan Li,<sup>b,c</sup> Yi Wang,<sup>a,1</sup> Baohong Guo,<sup>a</sup> Dong Han,<sup>a</sup> and Yuanjing Li<sup>a</sup>

<sup>a</sup>Key Laboratory of Particle and Radiation Imaging, Department of Engineering Physics, Tsinghua University, Beijing 100084, China

<sup>b</sup>State Key Laboratory of Particle Detection and Electronics, University of Science and Technology of China, Hefei 230026, China

<sup>c</sup>Modern Physics Department, University of Science and Technology of China, Hefei 230026, China

E-mail: [liu-jn20@mails.tsinghua.edu.cn](mailto:liu-jn20@mails.tsinghua.edu.cn)

**ABSTRACT:** This study focuses on developing a self-triggered data acquisition system and a noise reduction algorithm for the Multi-gap Resistive Plate Chamber (MRPC) Time-of-Flight Positron Emission Tomography (TOF-PET) system. The system integrates a fast front-end amplifier, a waveform digitization module based on the DRS4 chip, and an efficient noise reduction algorithm to address challenges such as high noise trigger rates and precise gamma-ray detection. The proposed self-triggered system, through threshold discrimination, coincidence logic, and continuous oscillation check, reduces the noise trigger rate to 0.004 Hz. Experimental results show that the system accurately localizes and images the  $^{22}\text{Na}$  radioactive source, and has a good time resolution of 162 ps FWHM for 0.511 MeV gamma rays.

**KEYWORDS:** Trigger concepts and systems (hardware and software); Resistive-plate chambers; Gaseous detectors

---

<sup>1</sup>Corresponding author.

---

## Contents

<b>1</b>	<b>Introduction</b>	<b>1</b>
<b>2</b>	<b>System setup and data acquisition</b>	<b>1</b>
<b>3</b>	<b>Self-triggered noise reduction algorithm</b>	<b>4</b>
<b>4</b>	<b>Positioning and imaging of <math>^{22}\text{Na}</math> radioactive source</b>	<b>7</b>
<b>5</b>	<b>Conclusion</b>	<b>10</b>

---

## 1 Introduction

The concept of Multi-gap Resistive Plate Chamber (MRPC) [1] Time of Flight (TOF) [2] Positron Emission Tomography (PET) is based on the detection principle of convert plates [3]. It takes advantage of the natural layered structure of MRPCs, their simple and low cost design, excellent time resolution [4], and remarkable position accuracy [5]. These features make MRPC TOF-PET particularly appealing for detailed imaging of small animals and high-sensitivity, whole-body TOF-PET imaging for humans. The Fonte team demonstrated imaging results using needle and planar  $^{22}\text{Na}$  sources, with the acquired data reconstructed through the Maximum Likelihood Expectation Maximization (MLEM) algorithm, achieving a stable and impressive resolution of 0.4 mm FWHM [6].

MRPCs are often used as TOF systems with data acquisition relying on scintillators for external trigger [7] in high-energy physics experiments. However, MRPC TOF-PET systems cannot use scintillators to trigger gamma ray detection. A self-triggered data acquisition system is needed to detect and record events of interest. High-performance commercial TOF-PET devices utilize tens of thousands of electronics channels to achieve high sensitivity and resolution [8]. The high noise trigger rate poses a significant challenge. This paper presented a self-triggered data acquisition system based on fast front-end amplifiers and waveform acquisition, along with an efficient noise reduction algorithm, aiming to enhance the accuracy of MRPC TOF-PET in detecting gamma rays. Experimental results show that the NTR of data acquisition using this self-triggered data acquisition system is significantly reduced, and the positioning and imaging results of the  $^{22}\text{Na}$  radiation source are accurate.

## 2 System setup and data acquisition

The self-triggered system primarily consists of MRPC detectors, fast front-end amplifiers, a waveform digitization module, and a data acquisition control terminal. The system setup is shown in figure 1. The MRPC prototype has 8 gas gaps with 0.128 mm gas gap thickness and 0.4 mm

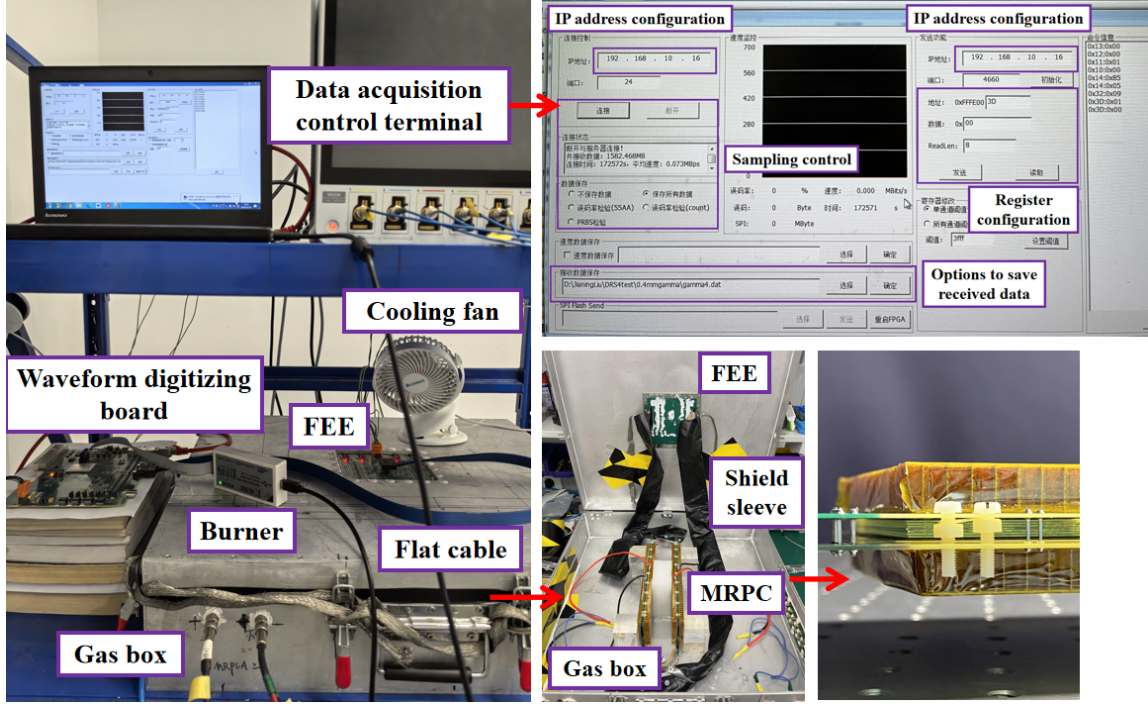
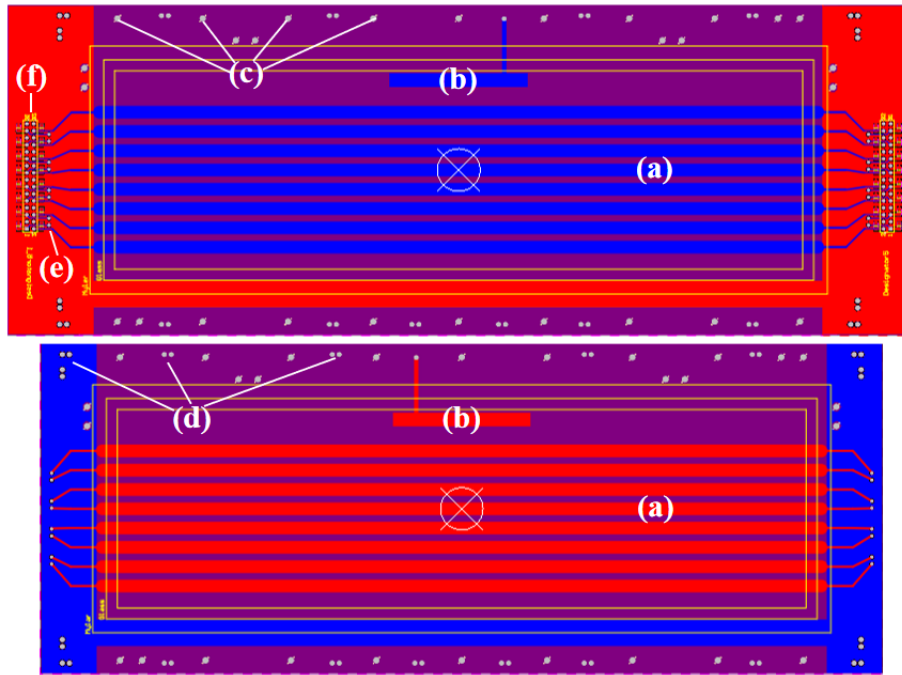


Figure 1. Test system diagram.

resistive plate thickness. Figure 2 shows the design of the Printed Circuit Board (PCB) for the MRPC prototype. Signals from the readout strips on the bottom PCB are transmitted to the top PCB through signal vias (e) and soldered pins. This design ensures that the transmission paths for the positive and negative polarity signals of the MRPC are identical. The differential signals generated by the MRPCs are then routed through differential signal output vias (f) and twisted-pair cables to the front-end electronics (FEE).

Hardware-level noise reduction optimizations have been implemented for signal readout. Differential readout is adopted, and input interfaces are equipped with ground vias. These ground vias help optimize the return path of signals and reduce the influence of external noise. Both sides of the PCB are copper-clad and connected to the ground. The front-end electronics are embedded in an aluminum gas box, with the MRPC detector's ground connected to the front-end electronics' ground. Signal transmission uses twisted-pair cables wrapped in aluminum foil shielding sleeves, as shown in figure 1. Utilizing twisted-pair cables to transmit signals to the electronics improves their noise immunity.

Our collaborator, the University of Science and Technology of China (USTC), completed the development of the fast front-end amplifier module and the waveform digitization module. Figure 3(a) shows the schematic diagram of the front-end amplifier module, which adopts a two-stage cascaded amplification structure. This design ensures low noise and high bandwidth while addressing the limitation of insufficient amplification gain in single-chip solutions. The first stage consists of coupling resistors and the LTC6430-20, a 20 dB ultralow-noise, high-bandwidth radio-frequency amplifier. The second stage uses the ADL5569, a 20 dB high-bandwidth operational amplifier. A 16-channel fast front-end amplifier board, as shown in figure 3(b), was fabricated. The



**Figure 2.** The design of the Printed Circuit Board (PCB) for the MRPC prototype. The labeled components in the figure are as follows: (a) Eight sets of readout strips, each with a width of 5 mm and a spacing of 2 mm; (b) High-voltage copper foil; (c) Holes for installing nylon posts used for winding fishing lines; (d) Mechanical fixing holes for soldering dual-row pins; (e) Signal transmission pinholes between the top and bottom PCB; (f) Differential signal output vias.

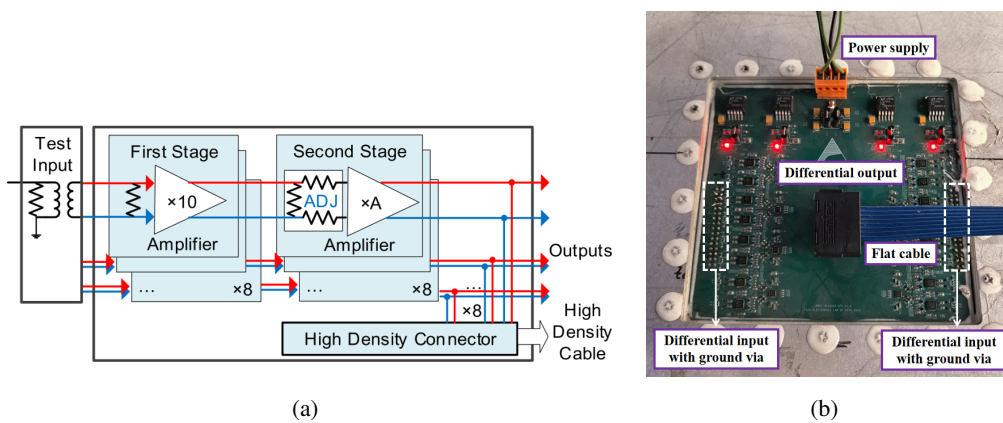


**Figure 3.** Front-end amplifier module. (a) Schematic diagram, (b) physical prototype.

input and output of the amplifier board are differential signals, with a configurable gain ranging from 20 to 100 times. The -3 dB bandwidth exceeds 1.4 GHz, and for input signals in the range of 5 mV to 50 mV, the time precision is better than 4 ps [9].

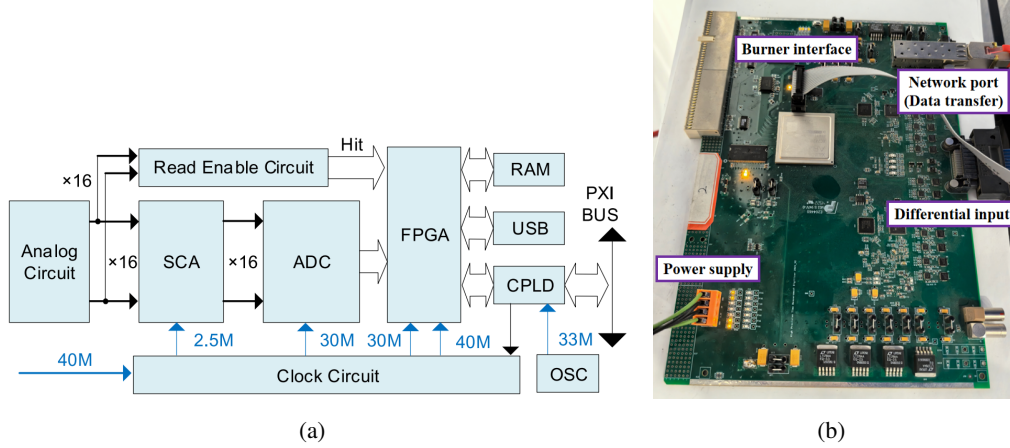


**Figure 4.** Waveform digitization module. (a) Schematic diagram, (b) physical prototype.

The structural schematic and physical prototype of the waveform digitization module are shown in figure 4. This module is designed based on the Domino Ring Sampler (DRS4) chip, Analog-to-Digital Converter (ADC) chip, and Field Programmable Gate Array (FPGA), and it includes analog front-end circuits, DRS4 waveform sampling circuits, analog-to-digital conversion circuits, and digital signal processing circuits. Signals from the front-end amplifier are buffered by an analog circuit to enhance the driving capacity of the sampling circuit and the readout enabling circuit. The signals are then continuously sampled and stored in the 1024 sampling capacitors of Switching Capacitor Array (SCA) chip called DRS4.

Once the signal exceeds the threshold of the readout enabling circuit, the stored charges are sequentially read out and fed into a 14-bit ADC, which digitizes them at a speed of 30 MHz for optimal linearity. After digitization, the ADC output data are input to the FPGA for further computation. The computed data can be transferred to a PC via the PXI bus through a Complex Programmable Logic Device (CPLD). The CPLD also configures the clock circuit and FPGA logic during power-up. This high-speed, high-precision waveform digitization board features 16 channels. Testing with sine waves and high-speed pulses demonstrates that the module operates at a sampling rate of 5.12 Gsps, with a -3 dB analog bandwidth of approximately 620 MHz. Additionally, its time resolution was verified by measuring the time difference of a high-speed pulse signal split into two parts. For input signal amplitudes ranging from 100 mV to 1 V, the single-channel time precision is better than 8 ps [9].

### 3 Self-triggered noise reduction algorithm

The signal waveforms read out by the MRPC detector using the fast front-end amplifier and the waveform digitization module when detecting 0.511 MeV gamma rays emitted by a  $^{22}\text{Na}$  radioactive source, are shown in figure 5. The rising time of the signal is defined as the time it takes for the

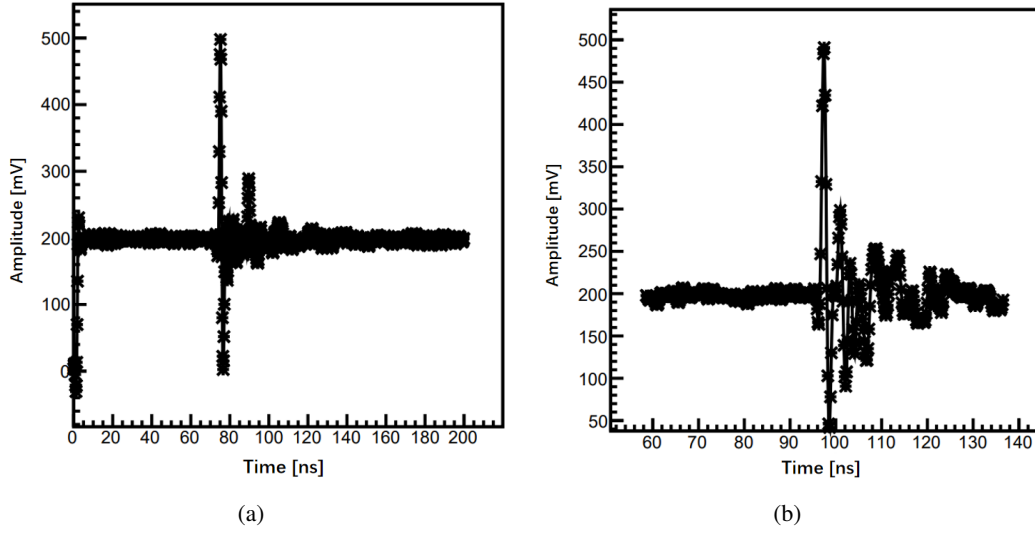


**Figure 5.** The waveform read out by the MRPC detector using the fast front-end amplifier and the waveform digitization module. (a) A complete signal waveform in the experiment, (b) local amplification of the waveform.

signal to rise from 10% to 90% of its maximum amplitude. The rising time of the output signal from the MRPC detector is approximately 0.5–1 ns, with a pulse width of about 1–2 ns. For the 8-gap MRPC with 0.128 mm gas gap thickness and 0.4 mm resistive plate thickness, the rising time distribution and amplitude distribution of signals detecting 0.511 MeV gamma rays are shown in figure 6. The average rising time of the signals is 502.1 ps, and the average signal amplitude is 299.3 mV.

The MRPC detector requires self-triggered to detect gamma rays. Figure 7 shows several complex waveforms captured using the waveform digitization module. In figure 7(a), the noise amplitude is relatively low, allowing low-amplitude noise signals to be preliminarily filtered out using threshold discrimination. Further, by applying logical coincidence checks, the system verifies whether signals in multiple channels simultaneously meet specific conditions, helping to distinguish noise signals from gamma events and reducing the system’s Noise Trigger Rate (NTR). The NTR refers to the frequency of false triggers caused by noise in the absence of valid signal inputs. It is a key metric for evaluating the noise immunity of the system. The NTR is defined as the number of noise-induced triggers per unit time, typically expressed using the following formula:

$$NTR = \frac{N_{noise}}{T} \quad (3.1)$$

where  $N_{noise}$  is the number of noise triggers within a certain time  $T$ , and  $T$  is the measurement time,  $NTR$  typically expressed in triggers per second (Hz). When the trigger threshold is set to 100 mV and the coincidence time window is 5 ns, under the condition that both MRPC detectors in the system satisfy the coincidence criterion of exceeding the threshold amplitude, the system’s NTR is 0.9 Hz.

To further reduce the system’s NTR and minimize the waste of data storage and processing resources, we introduced a continuous oscillation check during the data acquisition process. The



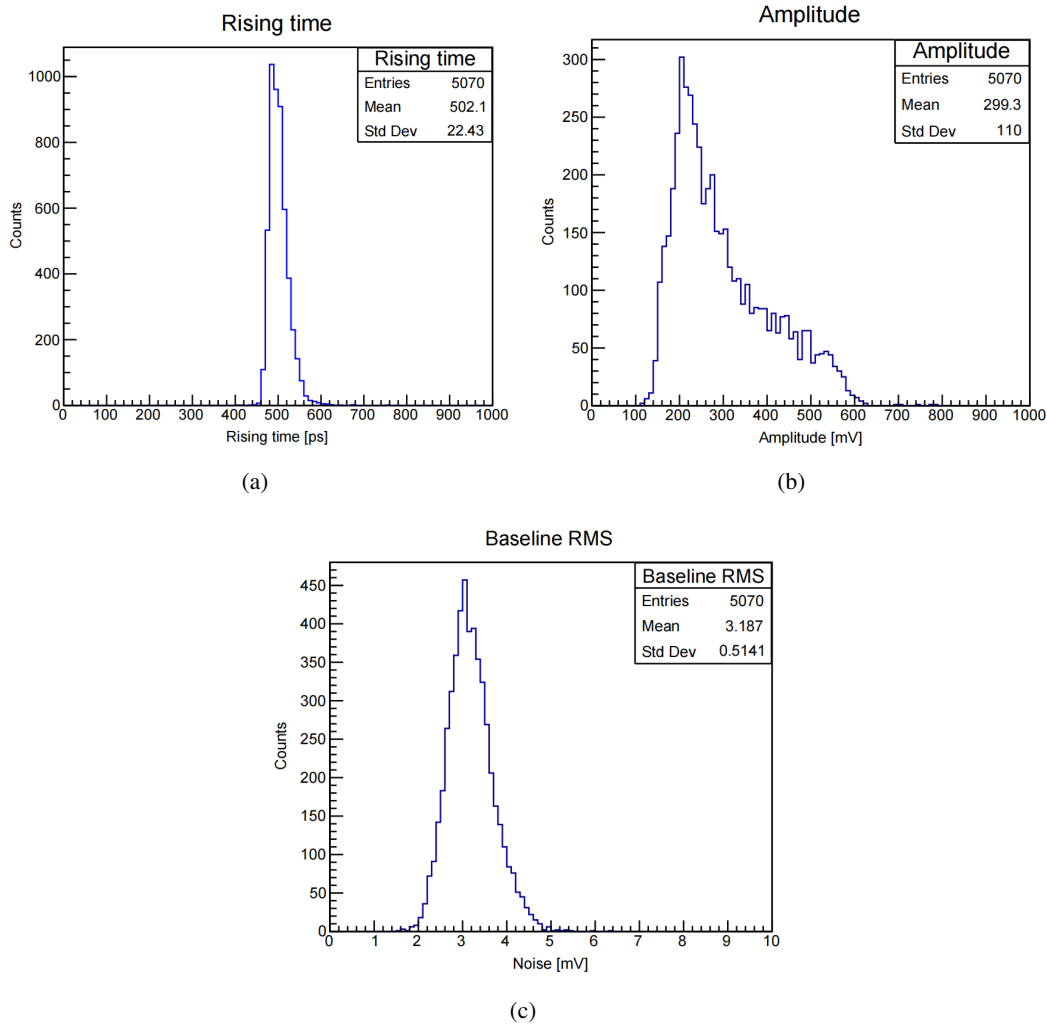


**Figure 6.** The signal characteristics of the 8-gap MRPC detecting 0.511 MeV gamma rays emitted by a  $^{22}\text{Na}$  radioactive source. (a) The distribution of signal rising time, (b) the distribution of signal amplitude, (c) the distribution of baseline RMS.

continuous oscillation check is based on the characteristic that noise signals often exhibit high-frequency, continuous oscillations, as shown in figure 7(b), whereas gamma event signals typically have specific waveform features. By counting the number of rising edges within 30 ns after the first rising edge, noise can be further eliminated. After applying the continuous oscillation check, the system's NTR was reduced to 0.004 Hz. The noise shown in figure 7(c) can be excluded by limiting the baseline Root Mean Square (RMS) value. The baseline RMS distribution of the 8-gap MRPC detecting 0.511 MeV gamma rays is shown in figure 6(c), with an average baseline RMS value of 3 mV. The noise shown in figure 7(d) can be eliminated by determining whether the amplitude of the first threshold-crossing peak is the maximum amplitude of the waveform.

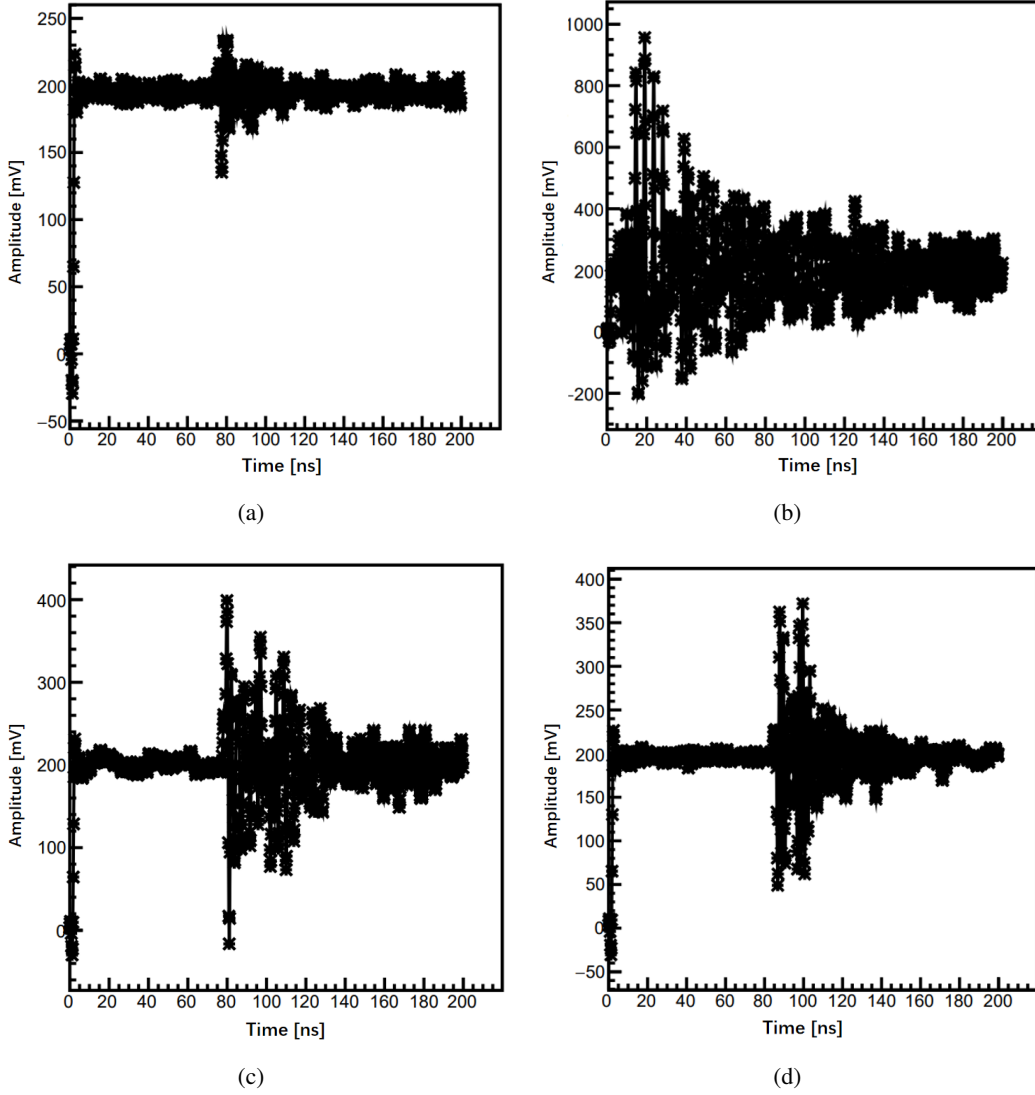


**Figure 7.** Examples of several complex waveforms from the 8-gap MRPC using the waveform digitization module.

#### 4 Positioning and imaging of $^{22}\text{Na}$ radioactive source

The physical diagram of the  $^{22}\text{Na}$  radioactive source used in the Gamma test is shown in figure 8(a). The diameter of the active area is 3 mm, and the activity is  $1.57 \times 10^5$  Bq. The definitions of the X, Y, and Z axes are shown in figure 8(b). The X-axis is defined as the direction perpendicular to the readout strips. The zero point of the X-axis is set at the midpoint of the 6th readout strip from the top down. The Y-axis is defined as the direction along the readout strips. The length of the readout strip is 264 mm, and the zero point of the Y-axis is set at the midpoint along the direction of the readout strip. The Z-axis is defined as the direction perpendicular to the MRPC detector plane. The zero point of the Z-axis is set at the center of the MRPC-C detector. The  $^{22}\text{Na}$  source is placed between MRPC-C and MRPC-B, 32 mm away from the MRPC-C detector and 40 mm away from



the MRPC-B detector. The position coordinates of the  $^{22}\text{Na}$  placement are (16 mm, 4.5 mm, 32 mm).

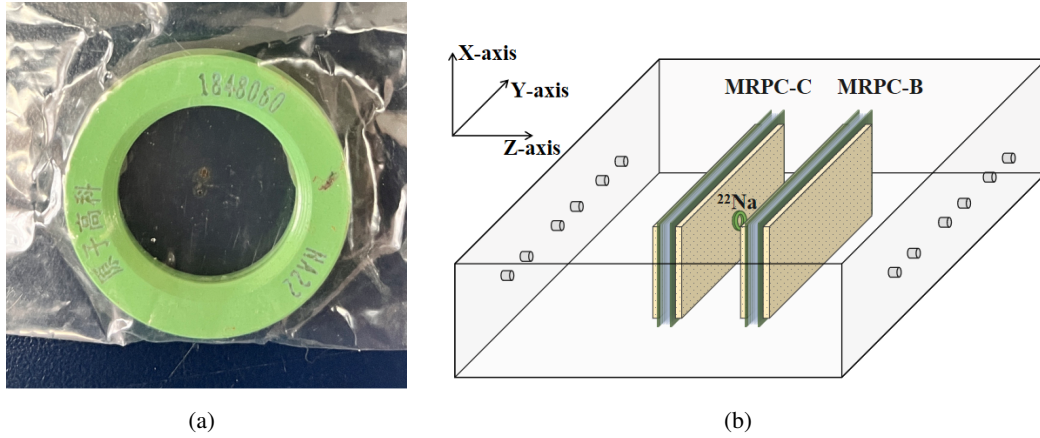


**Figure 8.** (a) Physical diagram of the  $^{22}\text{Na}$  radioactive source used in the Gamma test. (b) Schematic diagram of the definition of the X, Y, and Z-axis coordinates.

By measuring the induced signals on adjacent readout strips, and then using the Center of Gravity (COG) method, the position of the gamma interaction point perpendicular to the direction of the readout strip can be determined. The position of the gamma interaction point along the length direction of the readout strip is determined according to the time difference of the signals exceeding the threshold at both ends of the readout strip. After determining the positions of the interaction points of the gamma with the MRPC-C and MRPC-B detectors, a response line is drawn. Subsequently, the specific position on this response line is determined according to the time difference of this event between the two detectors. The Full Width at Half Maximum (FWHM) value of the time distribution calculated from the time difference between the two detectors is 162 ps, as shown in figure 9.

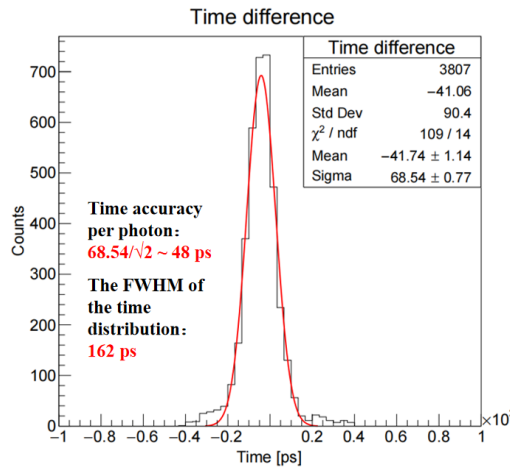


**Figure 9.** Distribution of the time difference in the Gamma test of the 8-gap MRPC detector.

The positioning points are presented as a three-dimensional image, as shown in figure 10(a).

The brown-red color represents the area where the positioning points are most concentrated. The projections of the positioning points in the X-axis, Y-axis, and Z-axis directions are shown in figure 10(b), (c), and (d) respectively. According to the Time-of-Flight (TOF) method, the coordinates of the  $^{22}\text{Na}$  source are located at (16.11 mm, 5.22 mm, 32.71 mm), and the  $\sigma$  values of the distributions in the X-axis, Y-axis, and Z-axis directions are 0.51 mm, 4.85 mm, and 5.26 mm respectively.

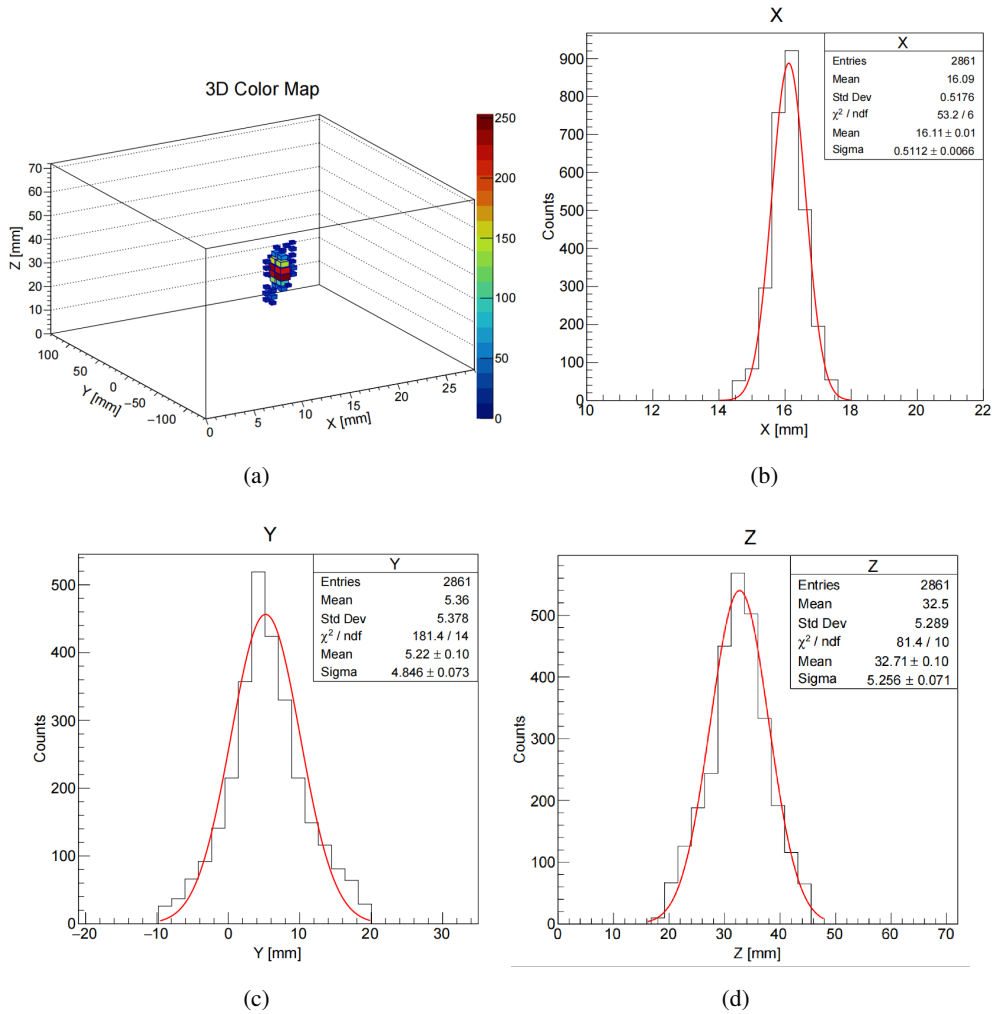


**Figure 10.** (a) Three-dimensional image of the  $^{22}\text{Na}$  source positioned by TOF and the projections of each positioning point in (b) the X-axis, (c) the Y-axis, and (d) the Z-axis directions.

In addition, we also positioned the  $^{22}\text{Na}$  source based on the intersection points of the response lines. The distribution of the response lines is shown in figure 11. A three-dimensional pixel map of the intersection points of the response lines is drawn, as shown in figure 12(a). The yellow color represents the area where the intersection points of the response lines are the most intensive. Ten pixel points are set per 1 mm. The projections of the distribution of the intersection points of the response lines in the X-axis, Y-axis, and Z-axis directions are obtained by conversion according to the three-dimensional pixel map, as shown in figure 12(b), (c), and (d). The position coordinates of the  $^{22}\text{Na}$  source positioned according to the intersection points of the response lines are (16.04

mm, 4.21 mm, 32.01 mm), and the  $\sigma$  values of the distributions in the X-axis, Y-axis, and Z-axis directions are 0.08 mm, 0.74 mm, and 1.08 mm respectively.

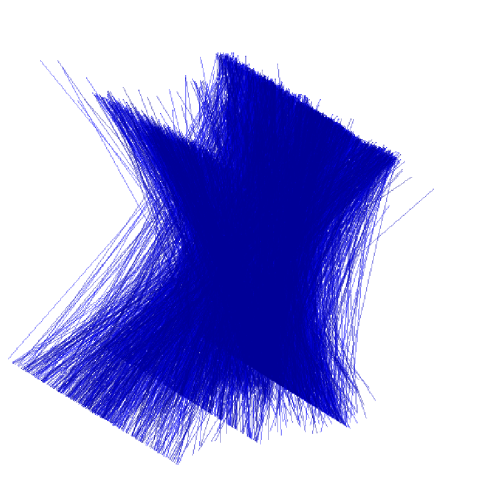


**Figure 11.** Distribution of response lines.

## 5 Conclusion

In this study, a self-triggered data acquisition system and an optimized noise reduction algorithm were developed for MRPC TOF-PET systems. The integration of a fast front-end amplifier and a DRS4 waveform digitization module enabled high-speed, high-precision signal processing. A multi-stage noise reduction strategy combining threshold discrimination, coincidence logic, and continuous oscillation check reduced the noise trigger rate to an ultra-low level of 0.004 Hz. The system demonstrated an excellent time resolution of 162 ps FWHM for 0.511 MeV gammas, enabling accurate results for both the localization and imaging of the  $^{22}\text{Na}$  radioactive source.

## Acknowledgments

The work is supported by the National Natural Science Foundation of China under Grant No. 11927901, 11420101004, 11461141011, 11275108, 11735009 and U1832118. This work is also supported by the Ministry of Science and Technology under Grant No. 2020YFE0202001, 2018YFE0205200 and 2016YFA0400100.

## References

- [1] E.C. Zeballos, I. Crotty, D. Hatzifotiadou, J.L. Valverde, S. Neupane, M. Williams et al., *A new type of resistive plate chamber: the multigap rpc*, *Nuclear Instruments and Methods in Physics Research Section A: Accelerators, Spectrometers, Detectors and Associated Equipment* **374** (1996) 132.
- [2] P. Fonte, A. Smirnitski and M. Williams, *A new high-resolution tof technology*, *Nuclear Instruments and Methods in Physics Research Section A: Accelerators, Spectrometers, Detectors and Associated Equipment* **443** (2000) 201.

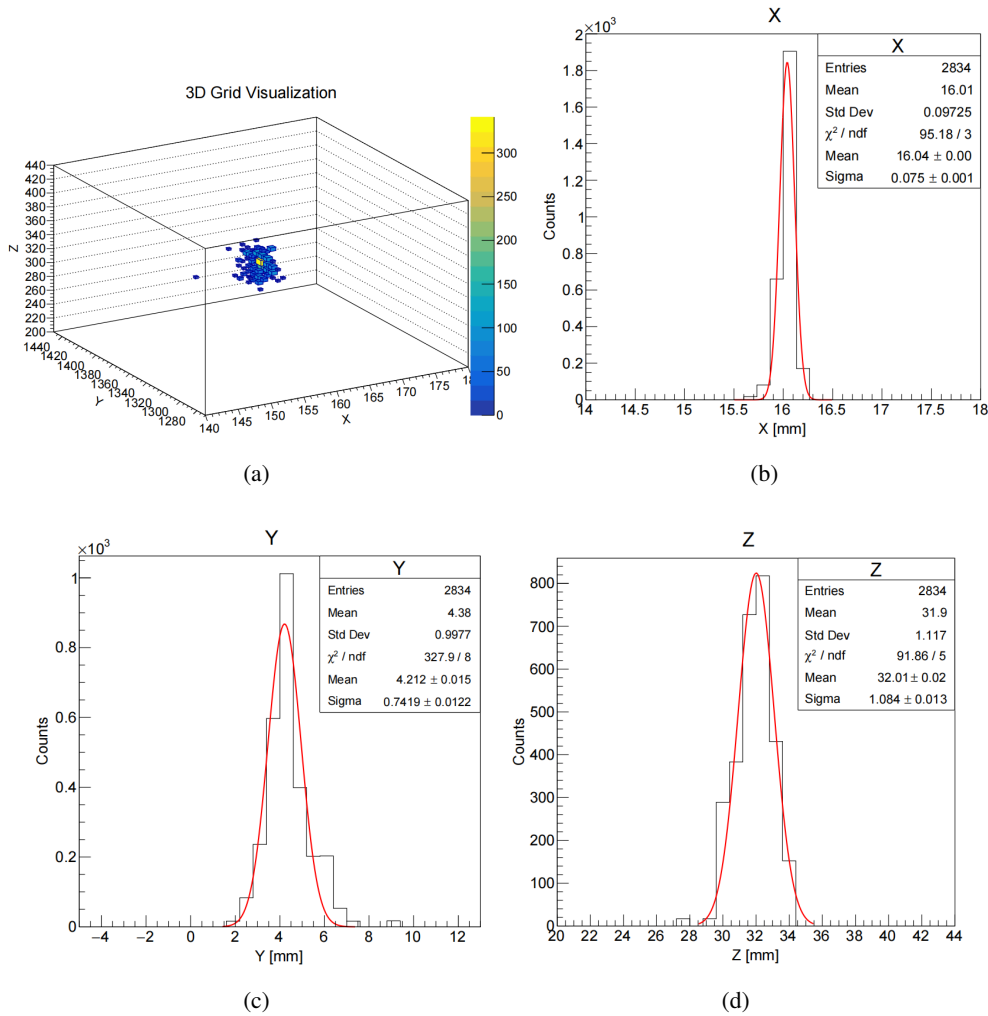


**Figure 12.** (a) Three-dimensional pixel map of the intersection points of the response lines and the projection distributions of the intersection points of the response lines in (b) the X-axis, (c) the Y-axis, and (d) the Z-axis directions, which are obtained by conversion from the three-dimensional pixel map.

- [3] J. Bateman, J. Connolly, R. Stephenson, G. Tappern and A. Flesher, *The rutherford appleton laboratory's mark i multiwire proportional counter positron camera*, *Nuclear Instruments and Methods in Physics Research* **225** (1984) 209.
- [4] J. Liu, Y. Wang, B. Guo, D. Han and Y. Li, *A very thin mrpc developed for tof-pet*, *Journal of Instrumentation* **19** (2024) C02068.
- [5] A. Blanco, P. Fonte, L. Lopes, P. Martins, J. Michel, M. Palka et al., *Toftracker: gaseous detector with bidimensional tracking and time-of-flight capabilities*, *Journal of Instrumentation* **7** (2012) P11012.
- [6] P. Martins, A. Blanco, P. Crespo, M.F.F. Marques, R.F. Marques, P.M. Gordo et al., *Towards very high resolution rpc-pet for small animals*, *Journal of Instrumentation* **9** (2014) C10012.
- [7] F. Wang, D. Han, B. Xie, Y. Wang, P. Lyu, B. Guo et al., *Performance study of a mosaic high rate mrpc*, *Journal of Instrumentation* **11** (2016) C09016.

- [8] B.A. Spencer, E. Berg, J.P. Schmall, N. Omidvari, E.K. Leung, Y.G. Abdelhafez et al., *Performance evaluation of the uexplorer total-body pet/ct scanner based on nema nu 2-2018 with additional tests to characterize pet scanners with a long axial field of view*, *Journal of Nuclear Medicine* **62** (2021) 861.
- [9] J. Liu, L. Zhao, L. Yan, Z. Li, S. Liu and Q. An, *Design of a prototype readout electronics with a few picosecond time resolution for mrpc detectors*, *Nuclear Instruments and Methods in Physics Research Section A: Accelerators, Spectrometers, Detectors and Associated Equipment* **925** (2019) 53.